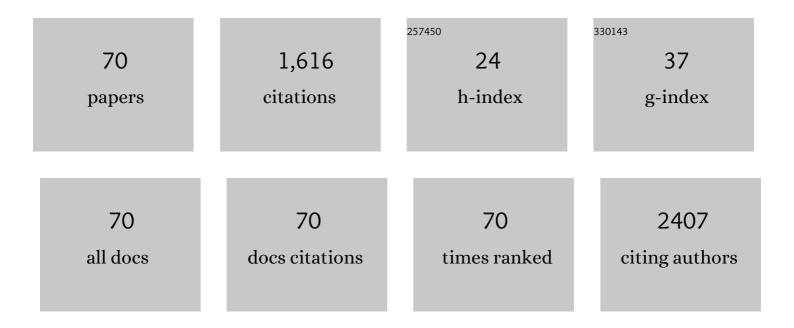
Mohammad Reza Mohammadi

List of Publications by Year in descending order

Source: https://exaly.com/author-pdf/1436724/publications.pdf Version: 2024-02-01



#	Article	IF	CITATIONS
1	Low-cost air-stable perovskite solar cells by incorporating inorganic materials. New Journal of Chemistry, 2021, 45, 788-795.	2.8	3
2	A single layer deposition of Li-doped mesoporous TiO2 beads for low-cost and efficient dye-sensitized solar cells. New Journal of Chemistry, 2021, 45, 2470-2477.	2.8	0
3	Performance of CoTiO ₃ as an oxide perovskite material for the light scattering layer of dye-sensitized solar cells. New Journal of Chemistry, 2019, 43, 3760-3768.	2.8	16
4	On the assessment of incorporation of CNT–TiO2 core–shell structures into nanoparticle TiO2 photoanodes in dye-sensitized solar cells. Photochemical and Photobiological Sciences, 2019, 18, 1840-1850.	2.9	14
5	Study of Hole-Transporter-Free Perovskite Solar Cells based on Fully Printable Components. Micromachines, 2019, 10, 266.	2.9	7
6	Solvent engineering based on triethylenetetramine (TETA) for perovskite solar cells processed in ambient-air. Photochemical and Photobiological Sciences, 2019, 18, 1228-1234.	2.9	4
7	Improvement of the photovoltaic parameters of perovskite solar cells using a reduced-graphene-oxide-modified titania layer and soluble copper phthalocyanine as a hole transporter. Physical Chemistry Chemical Physics, 2018, 20, 2388-2395.	2.8	40
8	Construction of Perovskite Solar Cells Using Inorganic Hole-Extracting Components. ACS Omega, 2018, 3, 46-54.	3.5	21
9	Carbon based perovskite solar cells constructed by screen-printed components. Electrochimica Acta, 2018, 276, 261-267.	5.2	41
10	Improving the stability of inverted perovskite solar cells under ambient conditions with graphene-based inorganic charge transporting layers. Carbon, 2018, 126, 208-214.	10.3	51
11	Enhanced electron collection efficiency of nanostructured dyeâ€sensitized solar cells by incorporating TiO ₂ cubes. Journal of the American Ceramic Society, 2018, 101, 293-306.	3.8	9
12	Long-term stability of dye-sensitized solar cells using a facile gel polymer electrolyte. New Journal of Chemistry, 2018, 42, 13256-13262.	2.8	28
13	The role of a vapor-assisted solution process on tailoring the chemical composition and morphology of mixed-halide perovskite solar cells. CrystEngComm, 2018, 20, 4428-4435.	2.6	7
14	Inverted perovskite solar cells based on lithium-functionalized graphene oxide as an electron-transporting layer. Chemical Communications, 2017, 53, 1630-1633.	4.1	40
15	Titania Nanotubes Decorated with Znâ€Doped Titania Nanoparticles as the Photoanode Electrode of Dyeâ€Sensitized Solar Cells. Energy Technology, 2017, 5, 1571-1578.	3.8	5
16	TiO ₂ –BaTiO ₃ nanocomposite for electron capture in dyeâ€sensitized solar cells. Journal of the American Ceramic Society, 2017, 100, 2144-2153.	3.8	33
17	Introduction of Graphene Oxide as Buffer Layer in Perovskite Solar Cells and the Promotion of Soluble n-Butyl-substituted Copper Phthalocyanine as Efficient Hole Transporting Material. Electrochimica Acta, 2017, 233, 36-43.	5.2	52
18	In-situ solvothermal processing of polycaprolactone/hydroxyapatite nanocomposites with enhanced mechanical and biological performance for bone tissue engineering. Bioactive Materials, 2017, 2, 146-155.	15.6	36

#	Article	IF	CITATIONS
19	Impact of chromium doping on physical, optical, electronic and photovoltaic properties of nanoparticle TiO ₂ photoanodes in dye-sensitized solar cells. New Journal of Chemistry, 2017, 41, 14516-14527.	2.8	12
20	Enhanced efficiency of over 10% in dye-sensitized solar cells through C and N single- and co-doped TiO2 single-layer electrodes. New Journal of Chemistry, 2017, 41, 9453-9460.	2.8	7
21	Plasmonic Effects of Infiltrated Silver Nanoparticles Inside TiO ₂ Film: Enhanced Photovoltaic Performance in DSSCs. Journal of the American Ceramic Society, 2016, 99, 167-173.	3.8	24
22	Impact of preparation method of TiO 2 -RGO nanocomposite photoanodes on the performance of dye-sensitized solar cells. Electrochimica Acta, 2016, 219, 38-48.	5.2	53
23	The beneficial effects of mixing spiro-OMeTAD with n-butyl-substituted copper phthalocyanine for perovskite solar cells. Electrochimica Acta, 2016, 222, 1417-1423.	5.2	21
24	A facile low temperature route to deposit a TiO2 scattering layer for efficient dye-sensitized solar cells. RSC Advances, 2016, 6, 70895-70901.	3.6	16
25	Soluble tetratriphenylamine Zn phthalocyanine as Hole Transporting Material for Perovskite Solar Cells. Electrochimica Acta, 2016, 222, 875-880.	5.2	41
26	Impact of Morphology and Nitrogen and Carbon Codoping on Photocatalytic Activity of TiO2 as Environmental Catalysts. Industrial & Engineering Chemistry Research, 2016, 55, 12205-12212.	3.7	11
27	Efficient dye-sensitized solar cells based on CNT-derived TiO ₂ nanotubes and Nb-doped TiO ₂ nanoparticles. RSC Advances, 2016, 6, 101737-101744.	3.6	10
28	Improved photon to current conversion in nanostructured TiO2 dye-sensitized solar cells by incorporating cubic BaTiO3 particles deliting incident. Solar Energy, 2016, 132, 1-14.	6.1	24
29	Effects of alumina nanoparticles concentration on microstructure and corrosion behavior of coatings formed on titanium substrate via PEO process. Ceramics International, 2016, 42, 8789-8797.	4.8	60
30	Efficient dye-sensitized solar cells based on carbon-doped TiO2 hollow spheres and nanoparticles. Journal of Materials Science: Materials in Electronics, 2015, 26, 8863-8876.	2.2	12
31	Design of TiO2 dye-sensitized solar cell photoanode electrodes with different microstructures and arrangement modes of the layers. Journal of Sol-Gel Science and Technology, 2015, 76, 666-678.	2.4	23
32	Development of an aqueous TiO2 paste in terms of morphological manipulation of nanostructured photoanode electrode of dye-sensitized solar cells. Journal of Sol-Gel Science and Technology, 2015, 75, 447-459.	2.4	5
33	Development of block copolymer-templated crack-free mesoporous anatase-TiO2 film: tailoring sol–gel and EISA processing parameters and photovoltaic characteristics. Journal of Materials Science: Materials in Electronics, 2015, 26, 1543-1553.	2.2	3
34	Improved Efficiency of Dye‣ensitized Solar Cells Based on a Single Layer Deposition of Skeinâ€Like <scp><scp>TiO</scp></scp> ₂ Nanotubes. Journal of the American Ceramic Society, 2014, 97, 2873-2879.	3.8	5
35	Double-layer dye-sensitized solar cells based on Zn-doped TiO2 transparent and light scattering layers: Improving electron injection and light scattering effect. Solar Energy, 2014, 103, 210-222.	6.1	61
36	Sensor Performance of Nanostructured TiO2–SnO2 Films Prepared by an Aqueous Sol–Gel Process. Journal of Cluster Science, 2014, 25, 905-923.	3.3	3

#	Article	IF	CITATIONS
37	Semiconductor TiO2–Al2O3 thin film gas sensors derived from aqueous particulate sol–gel process. Materials Science in Semiconductor Processing, 2014, 27, 711-718.	4.0	23
38	Double-Layer TiO2 Electrodes with Controlled Phase Composition and Morphology for Efficient Light Management in Dye-Sensitized Solar Cells. Journal of Cluster Science, 2014, 25, 1029-1045.	3.3	14
39	Study plasma electrolytic oxidation process and characterization of coatings formed in an alumina nanoparticle suspension. Vacuum, 2014, 108, 12-19.	3.5	63
40	Improved efficiency of dye-sensitized solar cells by design of a proper double layer photoanode electrodes composed of Cr-doped TiO2 transparent and light scattering layers. Journal of Sol-Gel Science and Technology, 2013, 67, 77-87.	2.4	21
41	Dependence of photovoltaic performance of solvothermally prepared CdS/CdTe solar cells on morphology and thickness of window and absorber layers. Journal of Materials Science: Materials in Electronics, 2013, 24, 3564-3574.	2.2	11
42	The improvement of electron transport rate of TiO2 dye-sensitized solar cells using mixed nanostructures with different phase compositions. Ceramics International, 2013, 39, 7343-7353.	4.8	22
43	Improved electron transportation of dye-sensitized solar cells using uniform mixed CNTs–TiO2 photoanode prepared by a new polymeric gel process. Journal of Nanoparticle Research, 2013, 15, 1.	1.9	14
44	Fuzzy local binary patterns: A comparison between Min-Max and Dot-Sum operators in the application of facial expression recognition. , 2013, , .		9
45	Synthesis of highly pure nanocrystalline and mesoporous CaTiO3 by a particulate sol–gel route at the low temperature. Journal of Sol-Gel Science and Technology, 2013, 68, 324-333.	2.4	16
46	Experiments design for hardness optimization of the Ni-Cr alloy electrodeposited by pulse plating. Acta Metallurgica Sinica (English Letters), 2013, 26, 558-564.	2.9	4
47	Controlling electron injection and electron transport of dye-sensitized solar cells aided by incorporating CNTs into a Cr-doped TiO2 photoanode. Electrochimica Acta, 2013, 111, 921-929.	5.2	27
48	Development of nanostructured porous TiO2 thick film with uniform spherical particles by a new polymeric gel process for dye-sensitized solar cell applications. Electrochimica Acta, 2013, 89, 90-97.	5.2	31
49	In vitro study of hydroxyapatite/polycaprolactone (HA/PCL) nanocomposite synthesized by an in situ sol–gel process. Materials Science and Engineering C, 2013, 33, 390-396.	7.3	89
50	Tailoring of morphology and crystal structure of nanomaterials in MgO–TiO2 system by controlling Mg:Ti molar ratio. Journal of Sol-Gel Science and Technology, 2012, 64, 135-144.	2.4	3
51	Synthesis and crystallization of lead–zirconium–titanate (PZT) nanotubes at the low temperature using carbon nanotubes (CNTs) as sacrificial templates. Advanced Powder Technology, 2012, 23, 647-654.	4.1	9
52	Development of hydroxyapatite nanorods-polycaprolactone composites and scaffolds derived from a novel in-situ sol-gel process. Tissue Engineering and Regenerative Medicine, 2012, 9, 295-303.	3.7	12
53	Concavity degree: A new feature for chromosome centromere localization. , 2012, , .		0
54	Low temperature nanocrystalline TiO2–Fe2O3 mixed oxide by a particulate sol–gel route: Physical and sensing characteristics. Physica E: Low-Dimensional Systems and Nanostructures, 2012, 46, 43-51.	2.7	20

#	Article	IF	CITATIONS
55	Dye-sensitized solar cells based on a single layer deposition of TiO2 from a new formulation paste and their photovoltaic performance. Solar Energy, 2012, 86, 2654-2664.	6.1	54
56	Tailoring of morphology and crystal structure of CdSe nanostructures by controlling the ratio of triethylenetetraamine and water in their mixed solution. Applied Physics A: Materials Science and Processing, 2012, 107, 497-502.	2.3	3
57	One-dimensional cadmium sulfide (CdS) nanostructures by the solvothermal process: Controlling crystal structure and morphology aided by different solvents. Materials Letters, 2011, 65, 1291-1294.	2.6	45
58	Controlling morphology and structure of nanocrystalline cadmium sulfide (CdS) by tailoring solvothermal processing parameters. Journal of Nanoparticle Research, 2011, 13, 3011-3018.	1.9	25
59	Preparation and characterization of nanocrystalline and mesoporous strontium titanate thin films at room temperature. Journal of Coatings Technology Research, 2011, 8, 585-593.	2.5	3
60	Synthesis of Nanostructured and Nanoporous TiO2-AgO Mixed Oxide Derived from a Particulate Sol-Gel Route: Physical and Sensing Characteristics. Metallurgical and Materials Transactions A: Physical Metallurgy and Materials Science, 2011, 42, 2481-2492.	2.2	7
61	Template-based growth of titanium dioxide nanorods by a particulate sol-electrophoretic deposition process. Particuology, 2011, 9, 161-169.	3.6	21
62	Sol–gel derived nanocrystalline and mesoporous barium strontium titanate prepared at room temperature. Particuology, 2011, 9, 235-242.	3.6	33
63	Synthesis and characterisation of nanosized TiO2–ZrO2 binary system prepared by an aqueous sol–gel process: Physical and sensing properties. Sensors and Actuators B: Chemical, 2011, 155, 568-576.	7.8	48
64	Low temperature nanostructured lithium titanates: controlling the phase composition, crystal structure and surface area. Journal of Sol-Gel Science and Technology, 2010, 55, 19-35.	2.4	34
65	Synthesis and characterisation of nanostructured neodymium titanium oxides by sol–gel process: Controlling the phase composition, crystal structure and grain size. Materials Chemistry and Physics, 2010, 122, 512-523.	4.0	14
66	Water-based sol–gel nanocrystalline barium titanate: controlling the crystal structure and phase transformation by Ba:Ti atomic ratio. Journal of Materials Science, 2009, 44, 4959-4968.	3.7	7
67	Low-temperature perovskite-type cadmium titanate thin films derived from a simple particulate sol–gel process. Acta Materialia, 2009, 57, 1049-1059.	7.9	30
68	Preparation and characterisation of nanostructural TiO2–Ga2O3 binary oxides with high surface area derived form particulate sol–gel route. Journal of Materials Science, 2007, 42, 4976-4986.	3.7	17
69	Synthesis of high surface area nanocrystalline anatase-TiO2 powders derived from particulate sol-gel route by tailoring processing parameters. Journal of Sol-Gel Science and Technology, 2006, 40, 15-23.	2.4	72
70	Preparation and characterisation of nanostructural TiO2–Er2O3binary oxides with high surface area derived from particulate sol–gel route. Materials Science and Technology, 2006, 22, 965-974.	1.6	17